PHILOSOPHICAL TRANSACTIONS OF THE ROYAL SOCIETY A MATHEMATICAL, PHYSICAL & ENGINEERING SCIENCES

Resonant Tunnel Diodes as Submillimetre-Wave Sources

E. R. Brown and C. D. Parker

Phil. Trans. R. Soc. Lond. A 1996 **354**, 2365-2381
doi: 10.1098/rsta.1996.0105

Resonant tunnel diodes as submillimetre-wave sources

By E. R. Brown and C. D. Parker

Lincoln Laboratory, Massachusetts Institute of Technology, Lexington, MA 02173-9108, USA

Resonant-tunnelling diodes (RTDs) are one of the only quantum-transport devices that operate effectively at room temperature, and are well known for their high-speed coherent generation and switching characteristics associated with the negative differential resistance (NDR) region. This paper addresses their capability as high-frequency coherent sources. Two types of sources will be addressed here: (i) quasi-sinusoidal oscillators connected to a resonant circuit, and (ii) relaxation oscillators connected to a high-frequency energy-storage element, such as a length of transmission line. To date, the highest-frequency sinusoidal oscillator was a waveguide-mounted InAs–AlSb RTD that performed up to 712 GHz. Transmission-line relaxation oscillators have been demonstrated only at microwave frequencies but show promise as submillimetre-wave sources. Their output waveform consists of a sequence of pulses having a repetition rate determined by the electrical delay of the transmission line and a pulse width determined by the switching time of the diode. Because they do not require DC-bias stability in the NDR region, they are quite amenable to power-combining techniques, such as parallel arrays, and could behave in an analogous manner to the atomic species in a mode-locked laser.

1. Introduction

(*a*) *Submillimetre-wave solid-state sources*

The submillimetre-wave region, defined here as 300 GHz to *ca.* 3 THz, has long been lacking in solid-state sources. The physical reasons for this are fairly well known. Electronic devices are always limited in frequency by some characteristic response time, be it a transit time, diffusion time or some form of relaxation time. For example, transistors are ultimately limited by the transit time associated with the middle terminal (i.e. the gate of a field-effect transistor or the base of a bipolar transistor). This holds true even in the recent types of high-speed heterostructure devices, such as the high-electron-mobility transistor or heterojunction bipolar transistor. The limiting response time is related to the more meaningful maximum frequency of oscillation, $f_{\max}$. At present the fastest transistors display an $f_{\max}$ of roughly 300 GHz. However, because of the precipitous drop in output power at frequencies approaching $f_{\max}$, transistors are now practical as sources only up to about 100 GHz, and it is unlikely that they will achieve submillimetre-wave operation in the near future.

At the opposite end of the submillimetre-wave spectrum, there has long been interest in developing solid-state lasers, such as junction-diode lasers using narrow-bandgap semiconductors. As shown in figure 1, diode lasers have been demonstrated

Phil. Trans. R. Soc. Lond. A (1996) **354**, 2365–2381
Printed in Great Britain

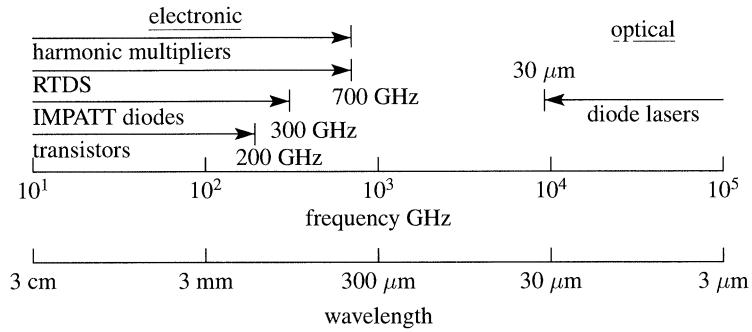

Figure 1. Solid-state source technology spanning the submillimetre-wave region.

out to wavelengths of about 30 μm, and there are many good proposals to develop solid-state lasers at even longer wavelengths using the strong intersubband transition in quantum-well structures (Capasso, this volume). However, all laser designs are frustrated by the natural increase in the spontaneous emission time and the associated decrease in the probability of stimulated emission with increasing wavelength. The most promising submillimetre-wave solid-state sources have been negative differential resistance (NDR) diode oscillators and varactor-diode harmonic multipliers. In general, diodes are more effective than transistors at these frequencies because of their simplicity. For example, IMPATT diodes have oscillated at fundamental frequencies up to about 300 GHz (Ino *et al.* 1977). In these diodes, the $f_{\max}$ is usually limited by a cancellation of the NDR by parasitic positive resistance in the device and the connecting circuit. The positive resistance tends to grow with frequency because of the skin effect in metals, radiative losses in transmission lines and interconnects, and dielectric relaxation in semiconductor epitaxial layers, among other factors. To avoid these problems, harmonic-multiplication techniques have been applied using powerful pump sources, such as klystrons or Gunn diodes, to pump varactor diodes around 100 GHz. While harmonic multiplication can be very efficient in doubling or even tripling, the efficiency falls rapidly at higher harmonic number because of the difficulty in properly terminating the harmonics below the desired one.

(*b*) *Resonant-tunnel diode*

The resonant-tunnelling diode (RTD) is a device that has gained considerable attention in recent years because of the strong NDR effect that it displays in many different material systems and over a very wide range of current density. In its simplest form, the RTD has the form shown in figure 2 consisting of two thin barriers (e.g. AlAs) of a semiconductor separated and clad by regions of a narrower bandgap semiconductor (e.g. GaAs). The critical factor in the RTD is that the region separating the barriers be thin enough to exhibit a strong quantum-size effect. In this case, electronic transport proceeds via resonant tunnelling through the metastable quantum state between the barriers, and the NDR occurs approximately when the bias drops this quantum state in energy below any occupied electron state on the injector (or cathode side) of the barriers.

In a practical sense, the RTD is remarkable because it is one of the few quantum-transport devices that operates at room temperature. This has facilitated its characterization at high speeds and has allowed the NDR region to be used for high-frequency oscillations and high-speed switching. For example, double-barrier RTDs made from the InAs–AlSb material system have oscillated up to 712 GHz (Brown *et al.* 1991),

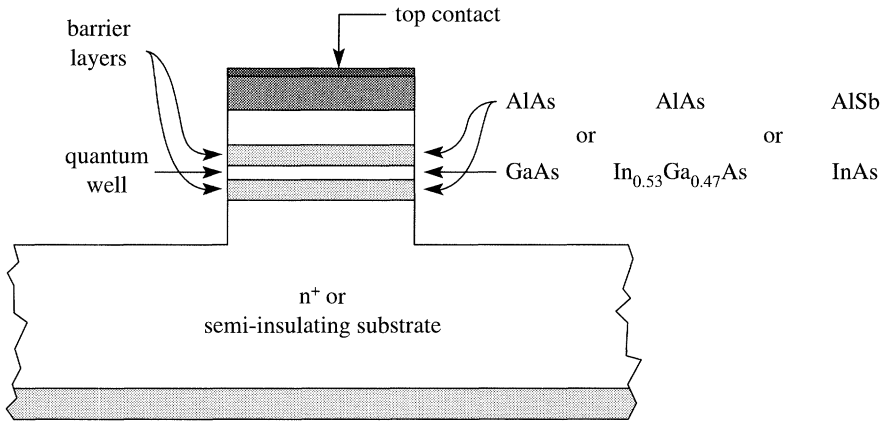

Figure 2. Cross-sectional view of a double-barrier resonant-tunnelling diode (RTD).

and similar diodes made from the GaAs–AlAs system have switched from the peak point to the valley region in a time near 2 ps (Whitaker *et al.* 1988). Much of the practical interest in RTDs stems from the fact that these results are among the highest oscillation frequencies and the lowest switching times reported to date for electronic devices.

2. High-speed RTD materials

(*a*) GaAs-*based materials*

The GaAs quantum well with $Al_xGa_{1-x}As$ barriers was the first resonant-tunnelling material system and remains an important one for high-speed RTDs since it is the simplest to grow and fabricate. In general, the thickness of the GaAs quantum well and AlGaAs barriers must be less than about 5 nm to observe the NDR effect at room temperature. Unfortunately, the best peak-to-valley current ratio (PVCR) values of *ca.* 4.0 occur with rather modest peak current densities in the range of *ca.* 1–5 $\times$ 10^4 A cm^{-2}. At the low end of this range, alloy barriers display the best characteristics, and at the upper end AlAs barriers are the best. At current densities above this range, the PVCR degrades significantly. For example, PVCRs of 1.4 and 2.5 have been achieved in RTDs having J_p of 1.5 $\times$ 10^5 A cm^{-2} (Brown *et al.* 1989*a*) and 1.5 $\times$ 10^5 A cm^{-2} (Diamond *et al.* 1989), respectively. This degradation is a drawback of GaAs–AlAs for the high-frequency-oscillator applications, which usually require $J_p \gtrsim 10^5$ A cm^{-2}. The *J*–*V* curve of a high-J_p GaAs–AlAs RTD developed at Lincoln Laboratory is shown in figure 3 in comparison with competitive material systems discussed below.

(*b*) $In_{0.53}Ga_{0.47}As$-*based materials*

The best material system in terms of PVCR and J_p is still $In_{0.53}Ga_{0.47}As$ (lattice-matched to InP) with $In_xAl_{1-x}As$ barriers. The lattice-matched barrier composition, $In_{0.52}Al_{0.48}As$, yields better PVCR at high current densities than GaAs. For example, a PVCR of 7 can be obtained at room temperature in samples having J_p up to *ca.* 10^5 A cm^{-2} (Sen *et al.* 1987; Lakhani *et al.* 1988). Nevertheless, better results can be obtained with barriers made of AlAs, which in the relaxed state has a 3.5% smaller lattice constant than $In_{0.53}Ga_{0.47}As$. If each AlAs barrier thickness is roughly 2.0 nm or less, it is pseudomorphic to $In_{0.53}Ga_{0.47}As$, and the resulting RTDs display very

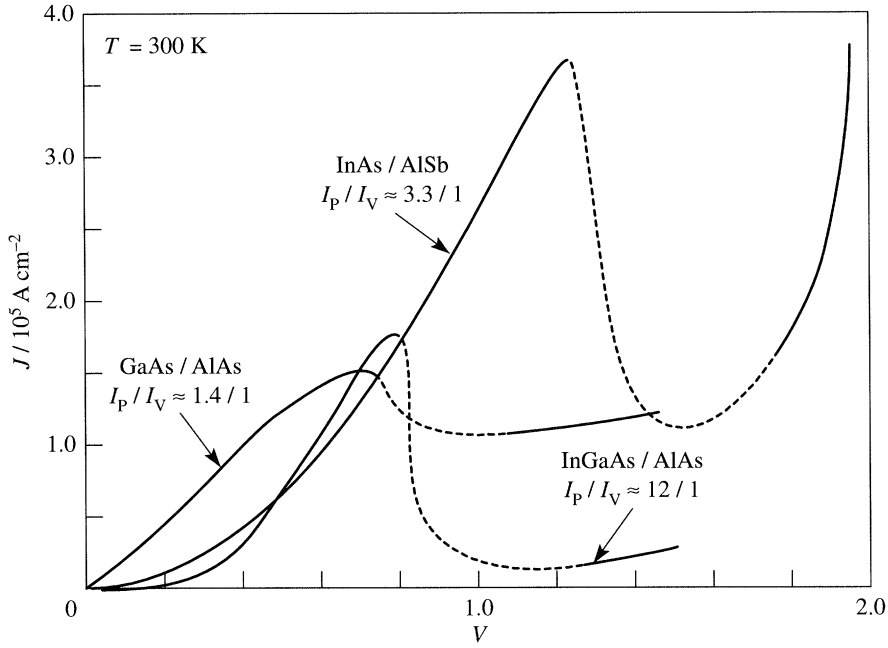

Figure 3. Current density versus voltage curves for high-speed resonant-tunnelling materials. The dashed segments are interpolations through the respective NDR regions.

high PVCR at high current density. The first such result was a PVCR of 14 at room temperature in a device with moderate J_p (Inata *et al.* 1987). Improvements in the growth technique have led to the RTDs having PVCR around 10 with J_p values in excess of 10^5 A cm^{-2}.

Other advantages of the $In_{0.53}Ga_{0.47}As$ RTDs over the GaAs-based systems include a much lower Schottky-barrier height (*ca.* 0.2 eV for common metals compared to *ca.* 0.8 eV for GaAs), and a greater solubility for the n-type dopants used in MBE. Both of these factors lead to a much lower series resistance for the InGaAs diodes, which is very important in high-speed devices.

(*c*) InAs-*based materials*

Perhaps the most intriguing high-speed material system studied to date consists of an InAs quantum well and cladding layers and AlSb barriers. It has a type-II staggered offset in which the valence band edge of the AlSb lines up in the gap of the InAs. Consequently, an electron tunnels into the AlSb from the InAs at an energy well below the maximum value of the attenuation coefficient, leading to a much higher transmission probability per unit barrier thickness than occurs in GaAs–AlAs or $In_{0.53}Ga_{0.47}As$–AlAs RTDs. This leads to superior current density with only a slight degradation in PVCR compared to the $In_{0.53}Ga_{0.47}As$–AlAs system. For example, the J–V curve in figure 3 applies to an RTD having 1.5 nm thick AlSb barriers and a 6.4 nm thick InAs quantum well (Söderström 1991). The values of $J_p = 3.7 \times 10^5$ A cm^{-2} and $\Delta J = 2 \times 10^5$ A cm^{-2} are comparable to the best results achieved in the $In_{0.53}Ga_{0.47}As$–AlAs system and are considerably better than those of the best GaAs–AlAs RTDs developed to date.

Aside from the advantageous band alignment of the InAs–AlSb system, the InAs itself has two other advantages related to high-speed device performance. First, elec-

trons will drift across a given depletion layer much more rapidly in InAs than in GaAs or $In_{0.53}Ga_{0.47}As$ provided that this layer is sufficiently thin (less than *ca.* 0.1 μm) or the voltage drop is small enough to maintain a low probability of impact ionization (Brennan & Hess 1984). This is because InAs has a much larger separation between the conduction band and the first upper valley than in GaAs or $In_{0.53}Ga_{0.47}As$. In addition, InAs has a weaker electron–longitudinal-optical phonon interaction than either material, and does not have the alloy-related scattering of $In_{0.53}Ga_{0.47}As$. A short depletion-layer transit time is necessary to achieve the highest speed. A second advantage is that the InAs RTDs have a significantly lower series resistance R_s that results primarily from the very low specific contact resistance ρ_c to InAs. A lower R_s also stems from the higher mobility of electrons in InAs than in GaAs or $In_{0.53}Ga_{0.47}As$ at any fixed n-type doping concentration.

(*d*) *Improved high-speed RTD*

An RTD material system that appears very promising but is difficult to realize is InAs quantum wells clad by GaAs or AlAs barriers. Even with GaAs, the barrier height should be great enough to suppress thermionic currents at room temperature. In addition, the small mass of the GaAs barrier would lead to a very small quasi-bound state lifetime for a given barrier thickness (Brown 1994). The combination of these factors should produce higher J_p and comparable PVCR to any of the above material systems for a given barrier thickness. The difficulty in realizing this system lies in the large lattice mismatch (greater than 7%) between InAs and GaAs or AlAs. This large mismatch hinders the epitaxial growth process at the interface between the two materials, leading to poor morphology and large defect concentrations in the top layer. Initial attempts to grow InAs–GaAs RTDs at Lincoln Laboratory (S. J. Eglash, personal communication 1992) were frustrated by these problems. However, very little of the growth phase space was explored in these experiments.

3. Sinusoidal oscillator

(*a*) *Principles of operation*

The physical basis for oscillations in RTDs is well known and follows, with only minor elaboration, from the principles of electrical oscillations in other N-type NDR devices, such as Esaki diodes. The essential conditions are (i) the DC bias is monostable, (ii) the AC load is unstable and (iii) the AC load circuit is resonant and has a loaded quality factor (including the RTD resistance) that exceeds unity at some frequency less than the f_{max} of the RTD. The first two conditions are given simply by $R_L < \Delta V/\Delta I$, where ΔV and ΔI are the width and height, respectively, of the NDR region, as depicted in figure 4. Under all three conditions, an AC fluctuation in the RTD voltage in the vicinity of the resonant frequency will grow exponentially until the amplitude roughly approaches ΔV. At this point, saturation sets in and a steady-state quasi-sinusoidal waveform occurs across the load resistor.

This simple picture of the RTD oscillation has proven very useful in understanding the important issues of maximum oscillation frequency and output power. In a study conducted in 1988, these issues were explained by way of the equivalent-circuit model displayed in figure 4. In this model, G is the differential conductance, C is the space-charge capacitance and L_{QW} is the quantum-well inductance, found from linear-response theory to be approximated by $L_{QW} = \tau/G$, where τ is the metastable-state lifetime. The f_{max} is the frequency at which the real part of the impedance looking

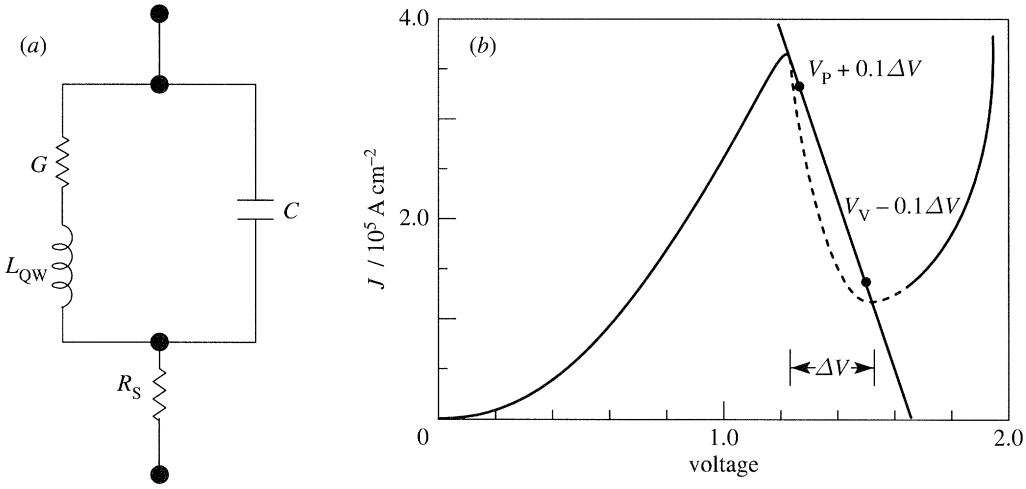

Figure 4. (*a*) Small-signal equivalent circuit diagram of double-barrier RTD. (*b*) Negative differential resistance characteristics of high-speed RTD.

into the device from the external terminals crosses from negative to positive, which has an interesting closed-form solution discussed elsewhere (Brown *et al.* 1989*b*). In the limit that $L_{QW} \rightarrow 0$ or equivalently $\tau \rightarrow 0$, this solution reduces to the result $f_{max} = (2\pi C)^{-1}[-G/R_s - G^2]^{1/2}$ derived first for Esaki tunnel diodes. One important feature of this expression is the presence of the series resistance R_s. As in all other NDR sinusoidal oscillators, reducing R_s generally increases f_{max}.

A variety of resonant circuits have been made with RTDs, but waveguide-based circuits have been the most useful for studying sinusoidal oscillators at high frequencies. One particularly effective circuit has been the quasi-optical resonator consisting of a waveguide-mounted RTD coupled to an open-cavity resonator, as shown schematically in figure 5. This circuit provides a higher quality factor at submillimetre-wave frequencies than an all-waveguide resonator, which in the simplest form is obtained from figure 5 by replacing the open cavity with a waveguide backshort. Details of the resonator design and performance are outside the scope of this paper, but can be found in the literature (Brown *et al.* 1992).

Oscillator results for waveguide-based RTDs made from the three high-speed material systems are presented in figure 6 along with lower-frequency results obtained from the same devices in coaxial resonators. All-waveguide oscillators were studied around 50, 100, 200, 350 and 650 GHz and quasi-optical oscillators were studied around 100 and 200 GHz. The first material system to operate in the submillimetre-wave region was GaAs with AlAs barriers. A 4 μm diameter device exhibited a maximum output power of *ca.* 15 μW at 112 GHz and 0.2 μW at 360 GHz, both from all-waveguide resonators. The $In_{0.53}Ga_{0.47}As$–AlAs diodes provided an absolute power of 50 μW at 110 GHz and 20 μW at 210 GHz, both from quasi-optical oscillators. This is the highest oscillation power obtained from an RTD to date above 100 GHz and is attributed both to the superior PVCR of the $In_{0.53}Ga_{0.47}As$–AlAs RTDs and to the superior characteristics of the quasi-optical resonator. The InAs–AlSb materials system remains the most promising one for submillimetre-wave oscillator applications. The absolute output power of a 2 μm diameter InAs–AlSb diode in an all-waveguide resonator at 360 GHz was 3 mW, which is about 12-fold more power than obtained from a GaAs–AlAs diode having four times the area. The highest frequency measured to

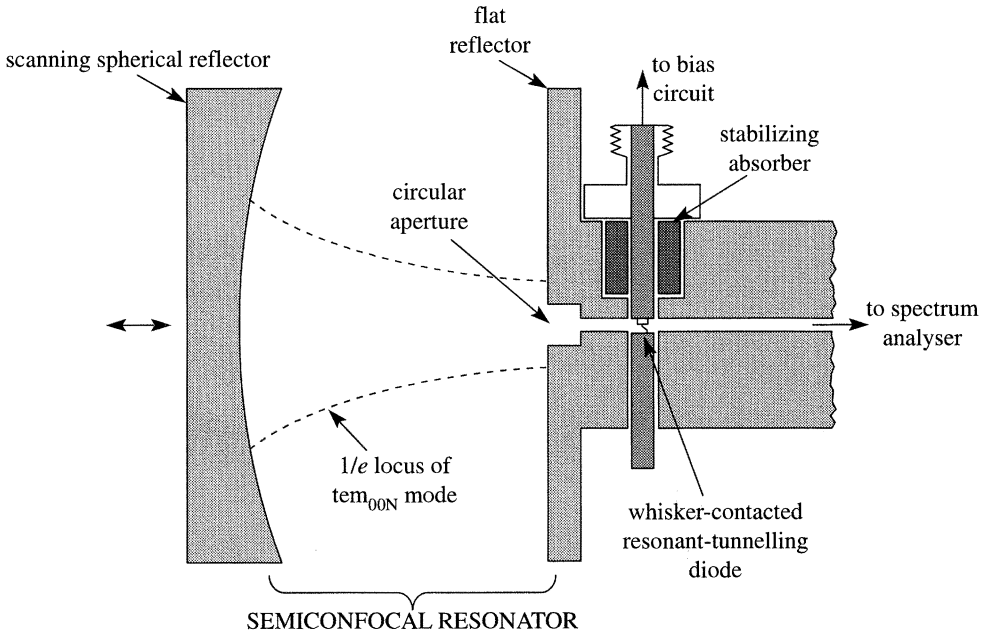

Figure 5. Quasioptical resonator used for the best RTD-oscillator results at frequencies above 100 GHz.

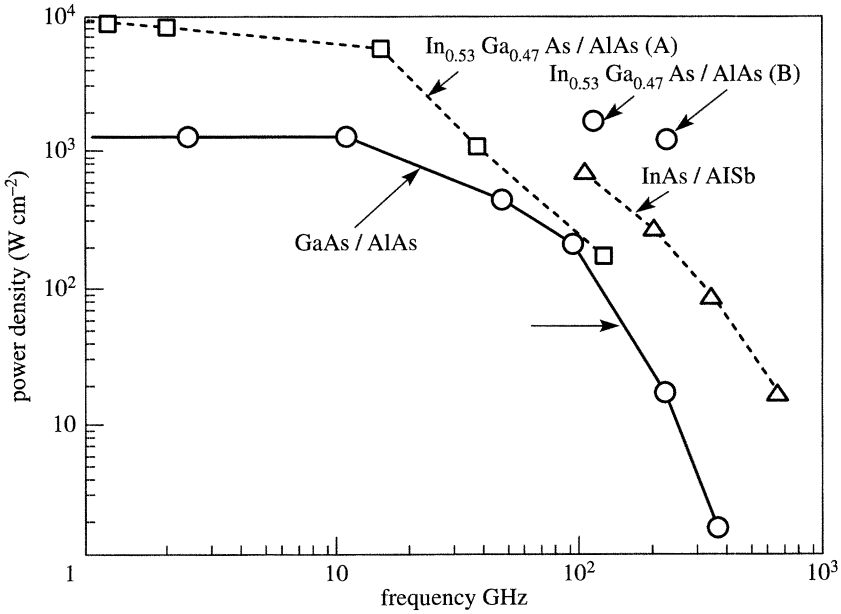

Figure 6. Sinusoidal oscillation results from RTDs made in the three high-speed material systems.

date from InAs–AlSb RTDs is 712 GHz (Brown *et al.* 1991). The power density and absolute power at this frequency were measured to be 20 W cm^{-2} and 0.5 μW, respectively.

The primary reason for the superior performance of the InAs–AlSb RTD is thought

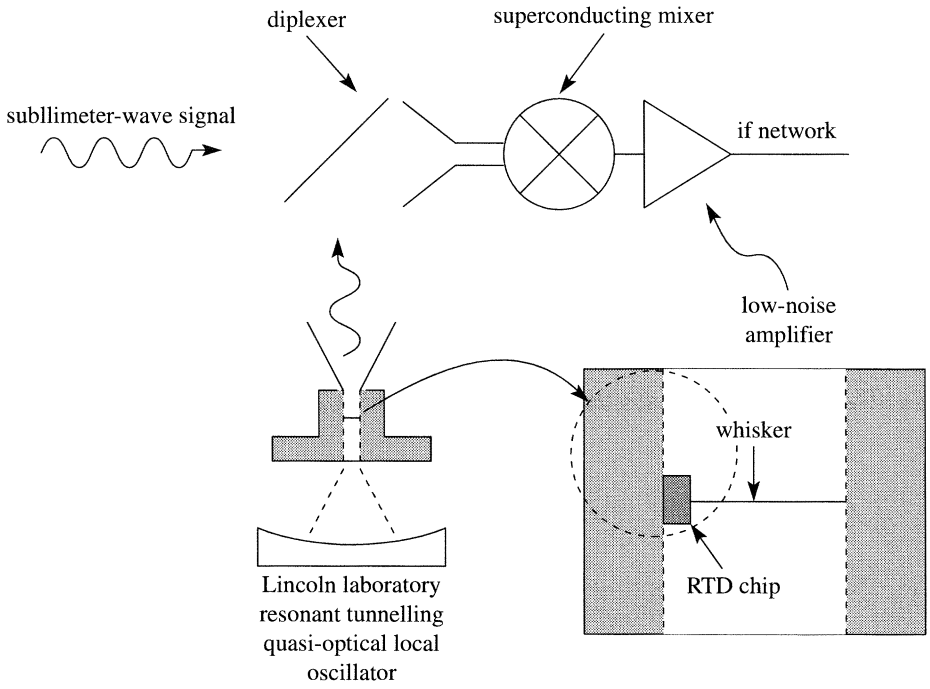

Figure 7. Schematic diagram showing application of sinusoidal RTD as a local oscillator in a superconducting-mixer-based radiometer.

to be the very low series resistance of the ohmic contact to n-InAs. In the present diodes the contact resistance is so low that its measurement is difficult, but we estimate from the oscillator results that its specific resistance is less than $2\times10^{-7}\ \Omega\ \mathrm{cm}^2$. A second reason for the superior performance, which is shared by the $In_{0.53}Ga_{0.47}As$–AlAs diodes, is the high available current density ($J_p - J_v \approx 3\times10^5\ \mathrm{A\ cm^{-2}}$). The power density from sinusoidal RTD oscillators is usually proportional to this quantity.

(*b*) *System application*

One of the most important applications of a THz solid-state source is as a local oscillator (LO) for radiometric receivers. With this application in mind, a candidate RTD oscillator has been characterized as an LO in conjunction with a working superconducting–insulator–superconducting (SIS) receiver at the Harvard–Smithsonian Institute in Cambridge, MA. A schematic diagram of the experimental set-up is shown in figure 7. The SIS receiver was designed to operate with low noise throughout the frequency range 220–270 GHz. The SIS mixer element, which was fabricated at the Institut de Radio Astronomie Millimétrique, consisted of two Al_2O_3 junctions in series, each having a normal resistance of 70 Ω. The receiver had an intermediate-frequency (IF) band centred at 4 GHz, an IF bandwidth of 1 GHz, and an IF noise temperature T_{IF} of *ca.* 11 K. Further details on the receiver are given in the paper by Blundell *et al.* (1992).

The RTD used in this experiment was an $In_{0.53}Ga_{0.47}As$–AlAs device with a room-temperature peak current density of $2.5\times10^5\ \mathrm{A\ cm^{-2}}$ and a PVCR of 9. With an input drive level of 2 V at 2 mA, output power levels were typically 20 μW over the range 194–215 GHz. This power level is adequate to pump a SIS mixer operating over the same frequency range.

Receiver noise measurements were made using the standard Y-factor technique with room-temperature (295 K) and liquid-nitrogen-cooled (77 K) loads placed alternately at the receiver input. Initial measurements were made using a frequency-doubled Gunn oscillator as the LO and with the diplexer set to minimum LO coupling. In this configuration a minimum receiver noise temperature of 125 K (double sideband) was measured at an LO frequency of 194.15 GHz. With the RTD oscillator as the LO, the diplexer had to be adjusted for 10% LO coupling to saturate the SIS mixer. Under this condition, the measured receiver noise temperature was 155 K. The 30 K difference increase with the RTD LO was attributable mostly to the stronger coupling required with the RTD. It was thus concluded that the RTD LO must have excess noise at least as low as the Gunn diode and that the RTD could be considered a viable candidate as an all-electronic LO in radiometric receiver applications.

4. Relaxation oscillator

(*a*) *Principles of operation*

The double-barrier RTD has one fundamental shortcoming for the sinusoidal oscillator application. The steep slope in the NDR region makes it very difficult to achieve DC bias stability in this region. Consequently, only small-area diodes having a suitably high differential resistance can be used. In the case of oscillators, the small area leads to a low output power relative to other two-terminal negative-resistance devices, such as Gunn and IMPATT diodes. To overcome this shortcoming, one must design either an RTD oscillator that does not require DC stability in the NDR region or a new type of RTD that provides a wider NDR region for greater ease of DC biasing in large-area diodes. The relaxation oscillator operates with a multistable DC-bias circuit, making it much easier start up the oscillator at the desired high frequency.

The relaxation oscillator is based on the repetitive switching of the RTD through the NDR region between DC-stable points lying below the peak point and above the valley point. To establish this type of oscillation, we imagine that the RTD is connected to one end of a short-circuited transmission line, as shown in figure 8. The transmission line has a characteristic impedance Z_0 and an electrical time delay t_d. The RTD is biased through a bias resistor R_B with a supply voltage V_B. The quiescent operation point is initially just below the peak or just above the valley and the RTD is induced to switch toward the valley or peak, respectively, by a slowly (e.g. manually) applied voltage ramp. Once the first switch occurs, a pulse travels down the line, is reflected from the short with inverted polarity, and arrives back at the RTD after a time $2t_d$. If $2t_d$ is sufficiently greater than the RTD switching time, then the return pulse will induce another RTD switch back to the initial operating point. The subsequent return pulse then induces a switch similar to the first one and the process repeats at a rate of approximately $(4t_d)^{-1}$. The overall process is classified as a relaxation oscillation because the RTD dwells in either of its positive differential resistance regions between switching events.

(*b*) *Microwave experiments*

The first high-speed relaxation oscillations were measured in the time domain using the schematic shown in figure 8. In this case, the RTD was a GaAs–AlAs device having an active area of approximately 40 μm^2, a peak current of 12 mA and a PVCR of 3.5 at room temperature. The RTD was series-mounted in a coaxial cartridge and its AC load resistor R_L was the 50 Ω input impedance of a sampling oscilloscope. The

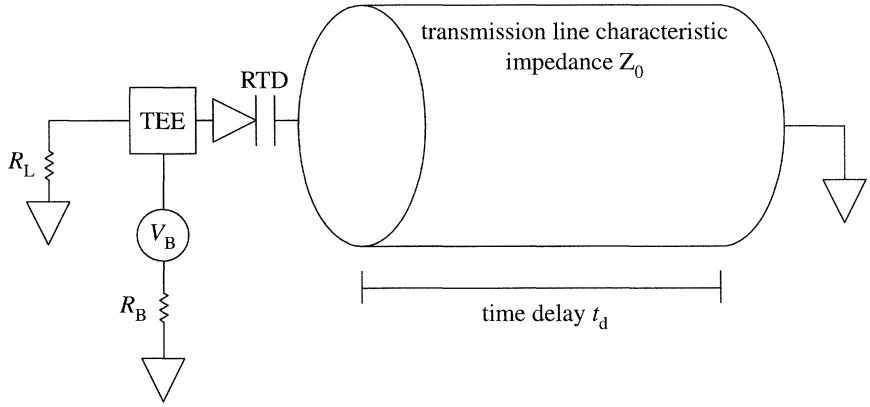

Figure 8. Schematic diagram of resonant-tunnelling transmission-line relaxation oscillator.

rise time of the oscilloscope was 25 ps. The bias voltage used to induce and maintain the oscillation was coupled to the RTD through a 40 GHz bias tee.

Shown in figure 9 is the output waveform of the device. It consists of alternating positive-going and negative-going pulses, corresponding to the RTD switching from the valley to the peak and from the peak to the valley, respectively. The positive-going amplitude is 0.25 V and the negative-going amplitude is 0.45 V. The negative switching event yields a greater voltage because it is associated with a greater change in current. The repetition rate is approximately 150 MHz. The pulse width at the 3 dB down point of both pulses is roughly 40 ps. This is limited mostly by the rise time of the sampling head. The highest-frequency repetition rate obtained with the pulse generator was about 3 GHz. In this case, the oscillating waveform looked quasi-sinusoidal rather than impulsive.

(*c*) *Numerical modelling*

A simple way to understand the relaxation-oscillator experiments and predict higher-frequency performance is by transient circuit simulation using the program SPICE3. The RTD is represented as a parallel combination of a nonlinear voltage-controlled current generator and a nonlinear capacitance. The voltage dependence of the current generator is chosen to be physically plausible, taking advantage of the trigonometric functions available in SPICE3E. The functional form is

$$I = A\{c_1 V[\arctan(c_2 V + c_3) - \arctan(c_2 V + c_4)] + c_5 V^n\}$$

where A is the area scale factor, the constants c_1 to c_4 are determined by the turn-on voltage, peak voltage, peak current and peak differential conductance of the RTD, and the constant c_5 is determined after obtaining c_1 to c_4 by fitting to the valley current and one arbitrary point beyond the valley. The exponent n is chosen to obtain a satisfactory fit to the overall I–V curve beyond the valley point. The two arctan terms occur in the stationary-state tunnelling theory of the RTD, with a Lorentzian form used for the transmission probability and a degenerate electron population assumed on the cathode side of the resonant-tunnelling structure. The degenerate electron population often occurs in high-speed RTDs. The polynomial term accounts for the excess current, which is the primary component beyond the valley point. Figure 10 shows the resulting RTD I–V curve with the parameters $c_1 = 0.0052$, $c_2 = 24.5$, $c_3 = 5.0$, $c_4 = 15.0$, $c_5 = 0.0014$ and $n = 5$. The resulting PVCR is 6.3, which is

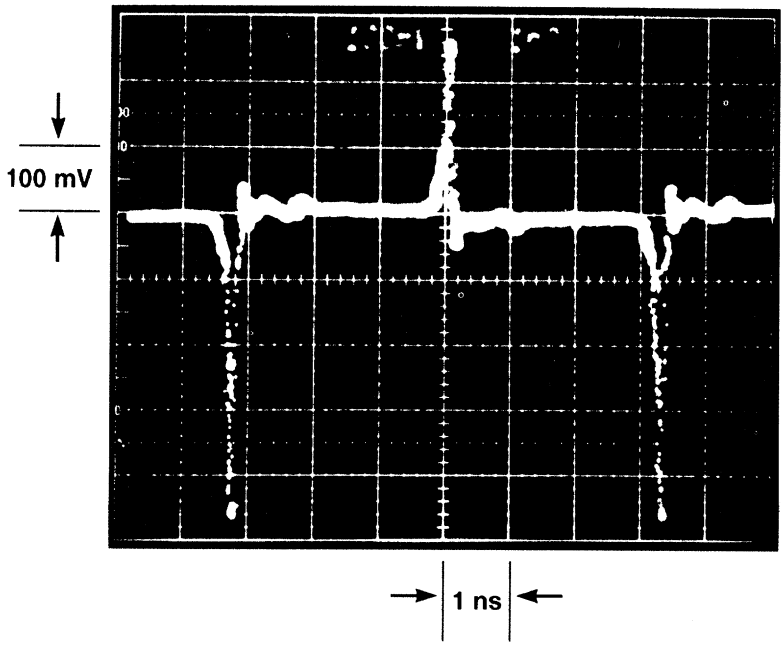

Figure 9. Experimental output waveform of relaxation oscillator.

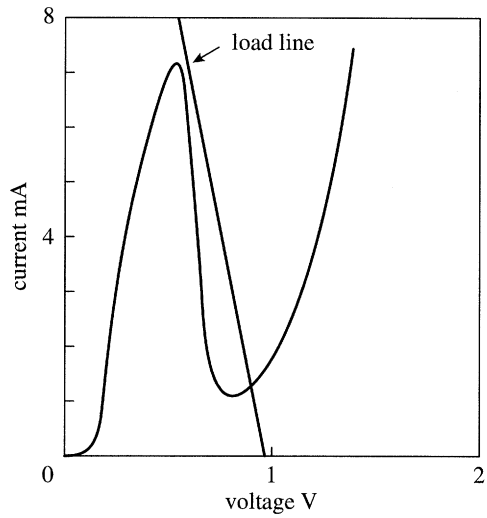

Figure 10. Model current–voltage curve and DC load line used in numerical simulations of RTDs at submillimetre-wave frequencies.

higher than the best GaAs–AlGaAs RTDs but lower than the best $In_{0.53}Ga_{0.47}As$–AlAs devices. The capacitance of the RTD is represented by a back-biased junction diode having the functional form $C = C_0(1 + V/V_j)^{-1/2}$.

The voltage difference across the load resistor is shown in figure 11 for four different transmission-line lengths (represented by the time delays) under the conditions $Z_0 = 50\,\Omega$, $R_B = 50\,\Omega$ and $V_B = 0.75$ V. A voltage ramp of magnitude 0.2 V and duration 50 ps is used to initiate the switching. In figure 11*a*, we see that $t_d = 0.9$ ps yields

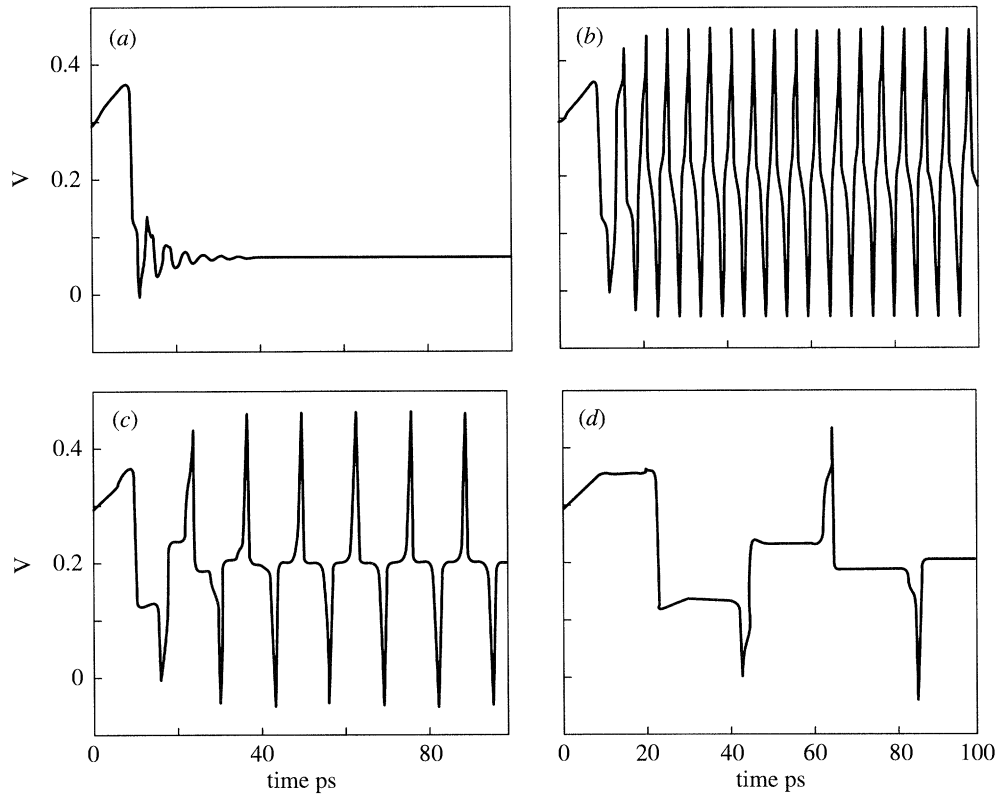

Figure 11. Relaxation-oscillator waveforms of voltage across the load resistor for transmission lines of varying electrical delay: (*a*) $t_d = 0.9$ ps, (*b*) $t_d = 1.0$ ps, (*c*) $t_d = 3.0$ ps, (*d*) $t_d = 10$ ps.

a single switching event followed by ringing around a low quiescent current point (just beyond the valley point of the RTD). The smallest t_d for which the switching is persistent is *ca.* 1.0 ps. In this case the waveform is periodic, as shown in figure 11*b*, but distinctly non-sinusoidal as shown by the impulsive nature of the voltage peaks. Oscillatory behaviour is also observed with the longer time delays of 3 ps in figure 11*c* and 10 ps in figure 11*d*. As observed experimentally, the waveform consists of a sequence of pulses of alternating polarity and of approximate repetition rate $(4t_d)^{-1}$. For both polarities, the pulse width is somewhat greater than the 10–90% switching time t_R of the RTD between the peak and valley points. An analytic expression for t_R is given by $4.4\Delta VC/\Delta I$, where ΔV is the difference between the valley and peak voltages, C is the capacitance at the peak point and ΔI is the difference between the peak and valley currents. For the present RTD we have $\Delta V = 0.28$, $\Delta I = 6.0$ mA and $C = 5.5$ fF, so that $t_R = 1.1$ ps. The lower value of t_R compared to the relaxation oscillator pulse width is caused by the fact that the oscillator switches over a wider voltage range, between the peak and a point approximately 0.4 V beyond the valley.

A useful way to interpret the results in figure 11 is by Fourier analysis. Shown in figures 12*a* and *b* are the discrete power spectra for the cases of $t_d = 1.0$ and 3.0 ps, respectively. At the fundamental frequency of 209 GHz, the relaxation oscillator generates 605 μW in the load resistor. Because of the impulsive nature of the output waveform, the third harmonic is quite strong with an output power of 78 μW, but the other harmonics are much weaker. In contrast, the power spectrum for $t_d = 3.0$ ps,

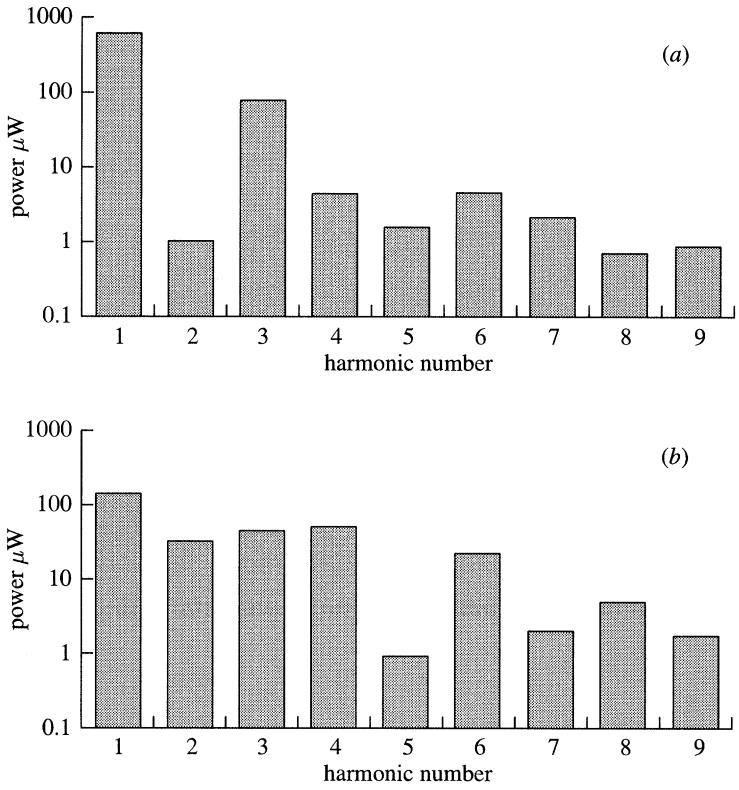

Figure 12. (*a*) Discrete power spectrum of relaxation oscillator simulated in figure 11*b*. (*b*) Discrete power spectrum of relaxation oscillator simulated in figure 11*c*.

plotted in figure 12*b*, shows much more uniform power with harmonic number. The fundamental of 88 GHz contains 140 μW of power, the fourth harmonic has 51 μW, and the sixth harmonic has 23 μW. This behaviour could have been anticipated from the distinctly impulsive nature of the waveform in figure 11*c*. In a sense, each output pulse is sharp enough to be approximated roughly as a delta function. The rich harmonic content then follows from the fact that a delta function in time corresponds to a uniform spectrum in the frequency domain.

Another way to characterize the difference between the two relaxation-oscillator spectra is by total harmonic distortion (THD), which is the sum of the power in all harmonics other than the fundamental divided by the power in the fundamental. For the waveform in figure 11*b*, THD = 39%, whereas for figure 11*c* THD = 106%. This leads to the following interesting concept. The relaxation oscillator operating in the impulsive regime may function as a very useful self-oscillating harmonic multiplier. For example, useful levels of power at several distinct frequencies in the submillimetre-wave region could be generated by coupling an RTD to a transmission line yielding a fundamental repetition frequency in the millimetre-wave region. This technique has two advantages. First, conventional transmission lines, such as metallic waveguides or coplanar lines on dielectric substrates, are much simpler to fabricate at millimetre-wave frequencies than multiplier circuits and have much lower loss. Second, varactive and electromechanical devices exist at millimetre-wave frequencies that would allow substantial tuning of the delay time and, hence, the repetition fre-

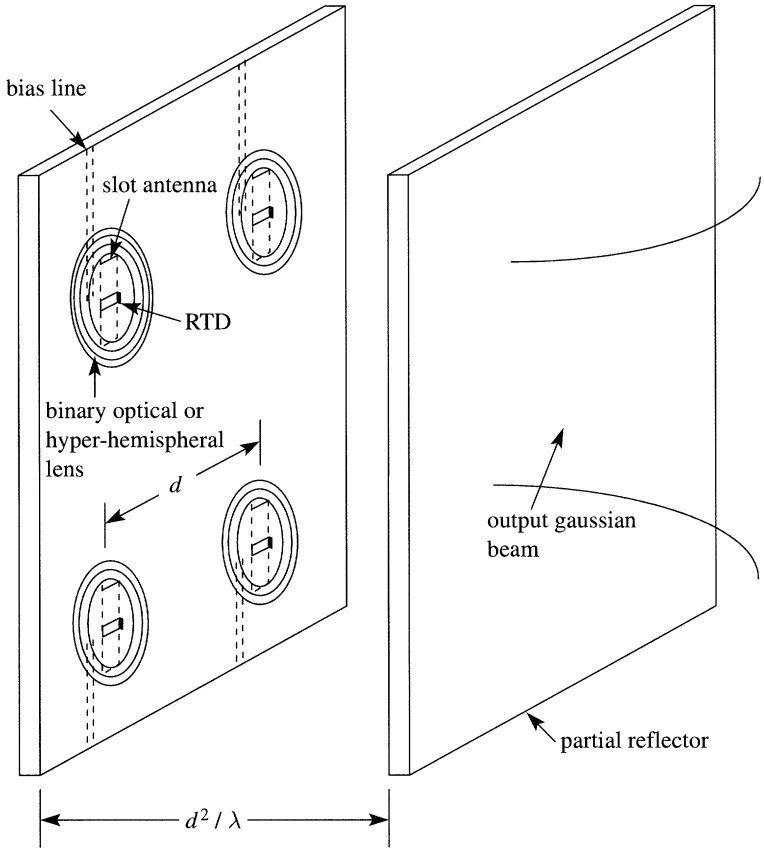

Figure 13. Diagram of two-dimensional array of relaxation oscillators coupled to an open cavity by the Talbot criteria.

quency of the relaxation oscillator. Of course, the submillimetre harmonics would tune much more, commensurate with their harmonic number.

(*d*) *Relaxation-oscillator array*

Most of the problem in obtaining useful power from sinusoidal RTD oscillators to date has been their limited size imposed by the DC-bias stability condition discussed above. Experience shows that high-speed RTDs fabricated in a large area (e.g. greater than or equal to 50 μm^2) will invariably oscillate on a spurious resonance in the bias circuit or not exhibit DC-bias stability in the NDR region at all. To alleviate this difficulty, it is necessary to fabricate oscillator arrays of small devices. Although there may be clever ways of fabricating these arrays in three dimensions, the two-dimensional planar approaches that have been proposed are all complicated by the fact that the DC-bias circuitry must not contain spurious resonances over practically the entire bandwidth below the desired sinusoidal oscillation frequency.

The relaxation-oscillator mode represents a much simpler way to combine the output power of two-dimensional planar arrays. The DC bias circuit feeding each RTD in the array need only satisfy $R_B > \Delta V/\Delta I$, which means that one circuit could conceivably feed many RTDs in the array. Like the sinusoidal-oscillator arrays, the relaxation-oscillator array would couple naturally to an open cavity, utilizing the fact

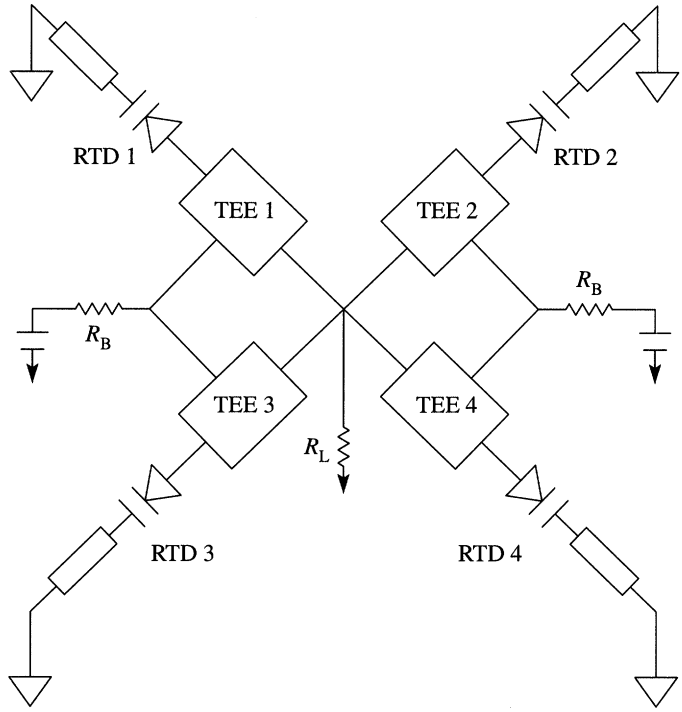

Figure 14. Equivalent-circuit diagram of relaxation-oscillator planar array.

that such a cavity represents a very low loss transmisison line for Gaussian beams propagating in free space.

A particularly attractive two-dimensional relaxation-oscillator array concept is that shown in figure 13. The RTDs are individually connected to a broadband planar antenna, such as a slot, and are separated from their nearest neighbours by distance d. The slots radiate into an open cavity separated from the plane of RTDs by the Talbot distance, d^2/λ. From physical optics, it is known that at this separation the intensity distribution in the plane of radiators will be replicated. Hence, a flat mirror located at this position will image the oscillator array back onto itself, leading to a strong coupling between neigbouring elements. This coupling will tend to synchronize the relaxation oscillators and yield a net output power approximately N times that of a single element where N is the total number in the array.

The behaviour of such an array has been simulated in SPICE3E using the same RTD model described above. The schematic diagram of the array is shown in figure 14 in which each RTD is assumed identical, as are the associated transmission lines. The net relaxation oscillator waveform for a five-element array is shown in figure 15 in comparison to that from a single element. The plotted quantity is the instantaneous power $I \times V$ across the common load resistor. Although there is no change in the amplitude of the load voltage, the current waveform is approximately five times greater, corresponding to a five-times increase in the output power at the fundamental and each harmonic.

In conclusion, note that there is an interesting analogy between the relaxation-oscillator array and a mode-locked laser. Both display an impulsive output power dictated by the round-trip time of radiation in some form of transmission line. Both involve repetitive switching or transitions between two stable states. In the mode-

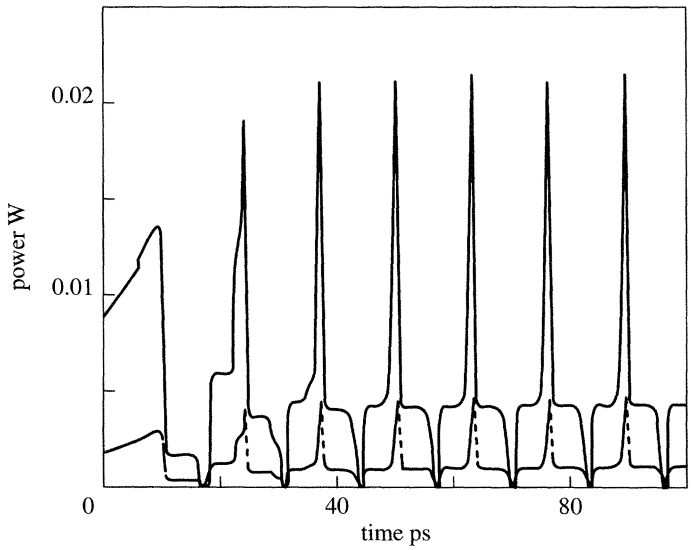

Figure 15. Simulated output waveform from relaxation-oscillator array having five elements.

locked laser, these are the upper and lower quantum states associated with photon emission or absorption. In the relaxation oscillator, the upper state is the quiescent bias point just below the peak and the lower state is the quiescent bias point just beyond the valley. And, finally, both display an output pulse width inversely related to the gain bandwidth of the transition. For the mode-locked laser, this is the spectral bandwidth of the stimulated-emission gain profile, For the relaxation oscillator, this is just the $f_{\max}$ of the RTD. This analogy is being pursued not only for physical insight but for design criteria, building on the wealth of engineering technique associated with optical mode-locked lasers.

5. Summary

Two modes of RTD oscillation have been addressed to ascertain their ability to generate coherent submillimetre-wave radiation. The sinusoidal-oscillation mode has generated the highest frequency measured to date, and with high-quality materials such as InAs promises coherent power up to approximately 1 THz. However, this mode is not viewed as readily supplying output power much beyond that already demonstrated (of the order of 1 μW). The second oscillation mode, the relaxation oscillator, is thought to be the stronger candidate for delivering more useful levels of power, perhaps of order 1 mW. This is because the relaxation oscillator does not require DC-bias monostability in the NDR region and, therefore, is relatively simple to combine in parallel two-dimensional arrays. Furthermore, because of its impulsive output waveforms, the relaxation oscillator is rich in harmonic content. Hence, it may serve well as a self-oscillating harmonic multiplier, similar in behaviour to a mode-locked laser.

References

Blundell, R., Miller, R. E. & Gundlach, K. H. 1992 *Electron. Lett.* **13**, 3.
Brennan, K. & Hess, K. 1984 *Solid-State Electron.* **27**, 347.

Brown, E. R. 1994 *Heterostructure and quantum devices* (ed. N. G. Einspruch & W. R. Frensley), pp. 306–347. Orlando, FL: Academic.

Brown, E. R., Sollner, T. C. L. G., Parker, C. D., Goodhue, W. D. & Chen, C. L. 1989*a* *Appl. Phys. Lett.* **55**, 1777.

Brown, E. R., Parker, C. D. & Sollner, T. C. L. G. 1989*b* *Appl. Phys. Lett.* **54**, 934.

Brown, E. R., Söderström, J. R., Parker, C. D., Mahoney, L. J., Molvar, K. M. & McGill, T. C. 1991 *Appl. Phys. Lett.* **58**, 2291.

Brown, E. R., Parker, C. D., Molvar, K. M. & Stephan, K. D. 1992 *IEEE Trans. Microwave Theory Technol.* **40**, 846.

Cheng, P. & Harris, J. S. 1990 *Appl. Phys. Lett.* **56**, 1676.

Diamond, S. K. Ozbay, E. Rodwell, M. J.W., Bloom, D. M., Pao, Y. C., Wolak, E. & Harris, J. S. 1989 *IEEE Electron Device Lett.* **10**, 104.

Inata, T., Muto, S., Nakata, Y., Fujii, T., Ohnishi, H. & Hiyamizu, S., 1987 *Japan. J. Appl. Phys.* **26**, L1332.

Ino, M., Ishibashi, T. & Ohmori, M. 1977 *Japan. J. Appl. Phys., Suppl.* **16-1**, 89.

Lakhani, A. A., Potter, R. C., Beyea, D., Hier, H. H., Hempfling, E., Aina, L. & O'Connor, J. M. 1988 *Electron. Lett.* **24**, 153.

Reddy, V. K., Tsao, A. J. & Neikirk, D. P. 1990 *Electron. Lett.* **26**, 1742.

Sen, S., Capasso, F., Hutchinson, A. L. & Cho, A. 1987 *Electron. Lett.* **23**, 1229.

Söderström, J. R., Brown, E. R., Parker, C. D., Mahoney, L. J. & McGill, T. C. 1991 *Appl. Phys. Lett.* **58**, 275.

Whitaker, J. F., Mourou, G. A., Sollner, T. C. L. G. & Goodhue, W. D. 1988 *Appl. Phys. Lett.* **53**, 385.

PHILOSOPHICAL TRANSACTIONS OF THE ROYAL SOCIETY A MATHEMATICAL, PHYSICAL & ENGINEERING SCIENCES